MAX-PLANCK-INSTITUT FÜR PHYSIK UND ASTROPHYSIK

MPI-PAE/Exp.El. 81
October 1979

Measurement of the baryon-exchange reactions $K^-p \to \Lambda\eta$, $K^-p \to \Lambda\pi^0$ at 6 GeV/c and the value of the ηNN-coupling constant

H. Becker[1], G. Blanar, W. Blum, J. de Groot[2], H. Dietl,
J. Gallivan, W. Kern[3], E. Lorenz, G. Lütjens,
W. Männer, D. Notz[4], R. Richter, T. Shimada,
U. Stierlin and M. Turala[5]

Max-Planck-Institut für Physik, München

and

V. Chabaud and R. Mount[6]

CERN, Geneva

ABSTRACT

In order to determine the ηNN coupling constant we have measured the two reactions $K^-p \to \Lambda\eta$ and $K^-p \to \Lambda\pi^0$ with a magnetic wire chamber spectrometer which contained a gamma counter for the $\gamma\gamma$-decays of π^0 and η. The Λ polarization and the differential cross-sections are given. The latter have quite different u-dependences. Their ratio is interpreted, in terms of a nucleon-Regge exchange model, as the effect of a small ηNN coupling constant for which we obtain $G^2_{\eta NN} = G^2_{\pi NN} \cdot (0.26 \pm 0.10)$ as allowed by SU_3. The large value given by Heisenberg's non-linear field theory, $G^2_{\eta NN} = G^2_{\pi NN} \cdot 0.9$, is excluded by this measurement if the characteristic u-dependence of the $\Lambda\pi^0$ channel is attributed to N_α Regge exchange.

October 1979

(Submitted to Nuclear Physics B)

---

1 Now at Fachhochschule Saarbrücken
2 Now at CERN, Geneva
3 Visitor from North-Eastern University, Boston, Mass., USA
4 Now at DESY, Hamburg
5 Visitor from Institute for Nuclear Physics, Cracow, Poland
6 Now at Nuclear Physics Laboratory, Oxford, U.K.

8000 MÜNCHEN 40 - FÖHRINGER RING 6

MAX-PLANCK-INSTITUT FÜR PHYSIK UND ASTROPHYSIK

Measurement of the baryon-exchange reactions $K^-p \to \Lambda\eta$, $K^-p \to \Lambda\pi^o$ at 6 GeV/c and the value of the ηNN-coupling constant

H. Becker[1], G. Blanar, W. Blum, J. de Groot[2], H. Dietl,
J. Gallivan, W. Kern[3], E. Lorenz, G. Lütjens,
W. Männer, D. Notz[4], R. Richter, T. Shimada,
U. Stierlin and M. Turala[5]

Max-Planck-Institut für Physik, München

and

V. Chabaud and R. Mount[6]

CERN, Geneva

ABSTRACT

In order to determine the ηNN coupling constant we have measured the two reactions $K^-p \to \Lambda\eta$ and $K^-p \to \Lambda\pi^o$ with a magnetic wire chamber spectrometer which contained a gamma counter for the $\gamma\gamma$-decays of π^o and η. The Λ polarization and the differential cross-sections are given. The latter have quite different u-dependences. Their ratio is interpreted, in terms of a nucleon-Regge exchange model, as the effect of a small ηNN coupling constant for which we obtain $G^2_{\eta NN} = G^2_{\pi NN} \cdot (0.26 \pm 0.10)$ as allowed by SU_3. The large value given by Heisenberg's non-linear field theory, $G^2_{\eta NN} = G^2_{\pi NN} \cdot 0.9$, is excluded by this measurement if the characteristic u-dependence of the $\Lambda\pi^o$ channel is attributed to N_α Regge exchange.

October 1979

(Submitted to Nuclear Physics B)

---

1 Now at Fachhochschule Saarbrücken

2 Now at CERN, Geneva

3 Visitor from North-Eastern University, Boston, Mass., USA

4 Now at DESY, Hamburg

5 Visitor from Institute for Nuclear Physics, Cracow, Poland

6 Now at Nuclear Physics Laboratory, Oxford, U.K.

8000 MÜNCHEN 40 - FÖHRINGER RING 6

1. INTRODUCTION

This experiment was designed to measure the ηNN-coupling constant by isolating and comparing the two nucleon-exchange processes shown in fig. 1a. The ratio of the differential cross-sections of this graph, extrapolated to the pole of the exchanged nucleon, is equal to the ratio of the ηNN- and πNN-coupling constants. The latter is well known from low-energy πN scattering and has the value $G^2_{\pi NN}/4\pi = 14.6$ [1]. The K^--induced processes of fig. 1a have a pure isospin $\frac{1}{2}$ exchange.

The numerical value of $G^2_{\eta NN}$ is presently unknown. There is the theoretical prediction from the non-linear field theory of Heisenberg and co-workers [2]: $G^2_{\eta NN} = G^2_{\pi NN} \cdot 0.9$. This theory also calculates $G^2_{\pi NN}/4\pi = 12.5$. On the other hand, the SU_3 symmetry of strong interactions predicts: $G^2_{\eta NN} = G^2_{\pi NN} \cdot \frac{1}{3}(3-4\alpha)^2$ [3]. This latter value depends on the ratio $\alpha = D/(D+F)$ of the symmetric octet coupling which may be taken to be $\alpha = 0.61$ (from the comparison of Σ and n leptonic decays using the Goldberger-Treiman relation [3]), or $\alpha = 0.60$ (the case of exact SU_6 symmetry [4]) or $\alpha = 0.66$ (from a Cabbibo fit to the hyperon beta decays [5]). For all choices of α in this range, the SU_3 prediction for $G^2_{\eta NN}/G^2_{\pi NN}$ is between 0.04 and 0.12. We have therefore two theories with conflicting predictions which are far enough apart to allow a decision to be made by experiment.

Previous attempts to determine $G_{\eta NN}$, based on analyses of low-energy nucleon-nucleon scattering in terms of one-meson-exchange forces (fig. 1b), are summarized in [1]. Results for $G^2_{\eta NN}/4\pi$ range between 0 and 10.2. They suffer from the difficulty of identifying the η in the forces between the nucleons.

Other attempts to determine $G_{\eta NN}$, based on the baryon exchange diagrams of fig. 1c, include the measurement of the backward-produced η and π^0 in the reactions $\pi^- p \to n\eta$, $n\pi^0$ by Chase et al. [6] and by Boright et al. [7]. If one assumes that these reactions are dominated by nucleon-exchange, one obtains $G^2_{\eta NN}/G^2_{\pi NN} = 0.18 \pm 0.06$ [6] and 0.45 ± 0.11 [7].

The difficulties here are mostly experimental because the final state ηn is not easily identified, and only cross-sections integrated over the backward production angles were given. This implies one did not really know the contribution of nucleon exchange. In addition, the exchanged baryons have both isospin $\frac{1}{2}$ and $\frac{3}{2}$ in the corresponding $N\pi$ reactions. Storrow and Winbow [8], and also Berger and Fox [9] have made comprehensive fits to all earlier πN backward scattering data. Whatever the most suitable model for the extrapolation to the nucleon-pole, it seems wise to avoid the $I_u = \frac{3}{2}$ contributions and to measure a lambda rather than a neutron in the final state if one wants to determine the relative strengths of the ηNN and πNN couplings.

In a high statistics bubble chamber exposure at 4.2 GeV/c, Marzano et al. [10] collected 18 events of the reaction $K^- p \to \Lambda\eta$ ($-u < 1.5$ GeV^2) and obtained $\sigma(\Lambda\pi)/\sigma(\Lambda\pi) = 0.18 \pm 0.06$ after integration over this backward region.

We report here on an experiment at the CERN PS using electronic counter techniques.

2. EXPERIMENTAL APPARATUS

The unseparated beam with 6.0 GeV/c momentum contained 1.4% K^-. The incident particles were measured and identified in the two arms of a magnetic spectrometer containing proportional wire chambers and Čerenkov-counters. The liquid-hydrogen target, 90 cm long, was surrounded by a γ-counter (cylindrical with an end-cap upstream) for the measurement of the $\gamma\gamma$ opening angles of the decays $\pi^o \to \gamma\gamma$ and $\eta \to \gamma\gamma$. The main magnetic wire chamber spectrometer measured the forward going Λ's through their charged decay products $p\pi^-$. A layout of the apparatus is shown in fig. 2. The trigger was designed to select a V^o in the forward direction decaying in front of the first wire chamber of the main spectrometer.

The spectrometers as well as the event reconstruction and acceptance calculation are described in more detail in the publication [11] of an experiment on the reactions $\bar{p}p \to \bar{\Lambda}\Lambda$,

$\bar{\Lambda}\Sigma^{o}$ and $\bar{\Lambda}$(missing mass) which were recorded simultaneously with the main experiment using the same trigger. As pointed out in [11], the event reconstruction and the acceptance calculation had to have small systematic errors due to the high statistical accuracy of the antiproton experiment.

The apparatus had a missing mass^2 resolution of σ = 0.07 GeV^2 on average, which may be compared to the difference $m_\eta^2 - m_\pi^2$ = 0.28 GeV^2. Only events with both Λ decay particles going through the magnet aperture were used, roughly 25% of those triggering, or 8% of those produced.

The γ counter was a position-sensitive lead-sandwich hodoscope with 27 strips along the beam direction. It allowed us to discriminate between the two channels $\Lambda\pi^{o}(\pi^{o} \to \gamma\gamma)$ and $\Lambda\eta(\eta \to \gamma\gamma)$ by measuring the opening angle ϕ between the two γ's. The technical details of this counter, the procedure for calibration and its general performance are published elsewhere [12]. Only between 44 and 55% (u-dependent) of the two-γ decays could be cleanly measured in two different strips, the rest had to be eliminated due to inefficiency, or simultaneous response to one γ of two neighbouring strips ("cross talk"), or because the two γ's hit the same strip. The overall efficiencies ε for clean measurement of a two-γ decay of η and π^{o} had a ratio $\varepsilon(\eta)/\varepsilon(\pi^{o})$ which was approximately independent of momentum transfer u due to the combined effects of cross talk and inefficiency. Typical measurement errors for the opening angle were $\sigma = 10^{o}$ (better for γ's with small angles to the beam axis, and worse if one γ had low momentum, but not exceeding 15^{o}). It may be noted that at a typical momentum transfer squared of u = 0.5, the minimum opening angle for π^{o}'s is 21^{o}, and 90% of the decays have $\phi < 46^{o}$; for η's, the two angles are 76^{o} and 121^{o}, respectively.

3. EXPERIMENTAL RESULTS

The events with a reconstructed Λ in the forward spectrometer and a K^- in the beam had the missing-mass^2 distribution shown in fig. 3a. After requiring "1,2 or 3 neutral signals"

in our gamma-counter, the resulting distribution was the one of fig. 3b. We finally obtained histogram 3c after a further restriction to events with exactly two separate γ's which also had to be coplanar with the missing momentum calculated from the incident K^- and the final Λ. To the right of the dominating π^o peak one observes signals due to η, ω and multi-π^o production.

Complete separation of the η- and π^o-signals is achieved by plotting the sample of histogram 3c in a scatter-diagram of missing mass^2 versus the $\gamma\gamma$ opening angle ϕ for various u-intervals, fig. 4. For each u, the energy E of the state with mass m decaying into $\gamma\gamma$ is fixed, hence in the ϕ distribution there is a sharp maximum at the minimal value $\phi_{min} = 2 \text{ arc } \sin(m/E)$ and a tail extending to 180^o. The boxes in fig. 4 are delimited by $\phi = \phi_{min} - 25^o$ (to accomodate the measuring error) and $\phi = \phi_{90}$, the value below which one has 90% of all ϕ's; the limits in m_x^2 are $\pm$ 2.2 σ around the square-masses of π^o or η; the boxes contain 87% of the $\pi^o \to \gamma\gamma$ and $\eta \to \gamma\gamma$ decays.

The numbers of events found in the boxes of the scatterplots are summarized in table 1. The fifth column contains the ratios of col. 4 multiplied by the ratio of the gamma counter and spectrometer detection probability which is slightly u-dependent. In col. 6 one finds the ratios of col. 5 multiplied by the ratio 2.60 of the branching ratios $(\pi^o \to \gamma\gamma/\pi^o \to \text{all})$: $(\eta \to \gamma\gamma/\eta \to \text{all})$ after a (14 $\pm$ 11)% background subtraction under the η-signal. Col. 6, therefore, represents the measured ratio of the differential cross sections of $K^-p \to \Lambda\eta$ and $\Lambda\pi^o$ at 6 GeV/c. The background subtraction is an attempt to interpolate the events with m_x^2 around m_η^2, which have opening angles outside the box, into the region of the η-signal. Such events may be $\Lambda\pi^o\pi^+\pi^-$, $\Lambda\pi^o\pi^o$, $\Sigma^o\pi^o$ etc., apart from $\Lambda\pi^o$(tail). The gamma-counter signals and Monte-Carlo techniques were used for the background subtraction, which is usually smaller than the statistical errors.

The differential cross section of the $\Lambda\pi^o$ reaction is plotted in fig. 5a, see also table 2. It exhibits the well-known shape with a maximum in the backward π^o direction and a minimum near $-u = 0.25$ GeV^2 which is characteristic for nucleon exchange. Comparing with other authors [10,13], the differential cross-section measured at 4.2 GeV/c [8] is the same within statistics up to a factor of 2.7 whereas the data at 5 GeV/c [13] show a more pronounced variation but are in rough agreement with our result, see fig. 6.

The differential cross section of the $\Lambda\eta$ reaction, fig. 5c, is derived from fig. 5a by multiplication with the numbers of col. 6, table 1. Its u-dependence bears no resemblance with the curve of the $\Lambda\pi^o$ reaction as it quickly falls from its maximum near $-u = 0.1$ as $-u$ increases; the two differential cross-sections are nearly equal between $u = 0$ and -0.3 GeV^2.

The integrated cross-sections are also listed in table 2, they include the over-all normalization error of ±10%. The ratio $\sigma(\Lambda\eta)/\sigma(\Lambda\pi^o)$ is .42 ± .08, confirming reference [7].

The polarization P of the Λ was measured through its decay asymmetry. As pointed out in [11] the u-dependent acceptance of the apparatus could be ignored because it was symmetric w.r.t. the horizontal median plane. For each u-interval we take $\alpha P = \Sigma \cos\theta_i / \Sigma \cos^2\theta_i$ with variance $1/\Sigma \cos^2\theta_i$ where θ is the angle between the proton direction of the Λ-decay and the normal to the production plane, $\bar{K}x\pi^o$, in the Λ rest frame. The summation extends over the events in each u-interval taken from the sample of fig. 3b with $m_x^2 < 0.14$ GeV^2, the asymmetry parameter α is +0.64 [14]. Fig. 5b depicts the variation of the measured Λ polarization with momentum transfer u. One observes it is nearly zero for small $|u|$ and negative, for $-u$ between ≈.1 and 1.1 GeV^2. The authors of [10] and [13] measured the same, inside their larger errors.

4. INTERPRETATION IN TERMS OF N_α- AND N_γ-REGGE TRAJECTORY EXCHANGE

The u dependences of the two differential cross sections being as different as shown in fig. 5, cannot be naively extrapolated to the nucleon pole to obtain the ratio $G^2_{\eta NN}/G^2_{\pi NN}$. Evidently we have different structures in the $\Lambda\eta$- and $\Lambda\pi$-amplitudes. In the framework of Regge theory, the characteristic dip-structure of the $\Lambda\pi$ cross-section is attributed to the exchange of the trajectory $N_\alpha(N^+_{1/2}(940), N^+_{5/2}(1688), N^+_{9/2}(2200), \ldots)$. The N_α Regge amplitude is zero at $j = \ldots\frac{7}{2}, \frac{3}{2}, -\frac{1}{2}, \ldots$, hence producing the minimum at $j = -\frac{1}{2}$ near $u = -0.15$ GeV. This behaviour is well known also in backward scattering of $\pi^+p \to p\pi^+$ and $\pi^-p \to n\pi^o$ whereas it is absent in $\pi^-p \to p\pi^-$ which cannot have an isospin $\frac{1}{2}$ trajectory exchanged.

The data of ref. [13] have recently been successfully interpreted by Papadopoulos and Resele [15] who included the N_γ-trajectory $(N^-_{3/2}(1520), N^-_{7/2}(2190), \ldots)$ as well, which was given a lower intercept than N_α. They were able to reproduce not only the shape of the $\Lambda\pi^o$ cross-section and the trend of the Λ-polarization at 5 GeV/c but also the $(I_u = \frac{1}{2})$ part of the $N\pi$ cross-section at 5.9 GeV [16,17], using SU_3-symmetric couplings. The contribution of $N_\beta(N^-_{5/2}(1670), N^-_{9/2}(2200), \ldots)$, the last one of the established isospin $\frac{1}{2}$ trajectories, was estimated to be extremely small due to EXD and SU_3. They had residue functions which eliminate three parity doublets on each trajectory.

Without invoking SU_3, we have made a two-parameter fit to the $\Lambda\pi^o$ differential cross-sections at 4.2, 5 and 6 GeV/c:

$$d\sigma/du(\Lambda\pi^o) = |x(1)\cdot N_\alpha(u,s) - x(2)\cdot N_\gamma(u,s)|^2 \qquad (1)$$

This is a short notation for the expression which contains the spinflip and noflip amplitudes explicitly:
$|x(1)\cdot N^f_\alpha(u,s) - x(2)\cdot N^f_\gamma(u,s)|^2 + |x(1)\cdot N^n_\alpha(u,s) - x(2)\cdot N^n_\gamma(u,s)|^2$, the Regge amplitudes as well as the relative sign between N_α, N_γ are the ones of ref. [13]+. The sign is essential for the

+ Our neglect of N_β is also justified because of the small branching ratio of $N^-_{5/2}(1670) \to \Lambda K$, independent of arguments relying on SU_3

polarization.

A similar two-parameter fit was produced for the linear combination $\frac{3}{2}(p\pi^+) + \frac{3}{2}(n\pi^o) - \frac{1}{2}(p\pi^-)$ which extracts the part of πN backward scattering with isospin $\frac{1}{2}$ exchange:

$$d\sigma/du(N\pi)_{\frac{1}{2}} = |x(3)\cdot N_\alpha(u,s) - x(4)\cdot N_\gamma(u,s)|^2 \qquad (2)$$

with the same N_α, N_γ[+]. The data at 5.9 and at 10 GeV/c were combined from [16] and [7].

Both fits are represented in fig. 6. Although the detailed u-dependence is not very accurately reproduced and despite a certain degree of dissimilarity between the data points of different experiments, we have a fairly good description of the shape and energy dependence of these baryon-exchange reactions with isospin $\frac{1}{2}$ exchange in terms of N_α and N_γ Regge poles. The fit parameters are listed in table 3.

Since our 6 GeV/c $\Lambda\pi^o$ data show a somewhat less dramatic cross-section variation with u indicating more N_γ at larger $|u|$ we have fitted them also to the form

$$d\sigma/du(\Lambda\pi^o) = |x(1)\cdot N_\alpha(u,s) - x(2)\cdot N_\gamma(u,s)\cdot(1-B\ u)|^2 \qquad (3)$$

with 3 parameters x(1), x(2), B. This clearly produces a curve which follows the data points more closely. These fits are used further down when comparing our $\Lambda\eta$ data to $\Lambda\pi^o$.

We will now interpret the $\Lambda\eta$ channel in terms of a superposition of N_α and N_γ exchange as well. (We have not included N_β because the leading member of N_β, $N^-_{5/2}(1670)$, is known to couple to $N\eta$ an order of magnitude more weakly than to $N\pi$). The ratio of cross sections is then given[++] by

---

[+] There are also kinematic factors which depend on the mass of the external particles.

[++] The kinematic factors were evaluated at the π-mass. The error introduced in R is less than 6%.

$$R(u) = \frac{d\sigma/du(\Lambda\eta)}{d\sigma/du(\Lambda\pi)} = \left| \frac{x(5)\cdot N_\alpha(u) - x(6)\cdot N_\gamma(u)}{x(1)\cdot N_\alpha(u) - x(2)\cdot N_\gamma(u)} \right|^2 \qquad (4)$$

where x(1), x(2) are taken from table 3 and x(5), x(6) are to be determined from our measured ratio R(u) listed in table 1. The ratio $x_\alpha = x(5)/x(1)$ represents the ratio of the ηNN_α over the πNN_α coupling strengths, the ratio $x_\gamma = x(6)/x(2)$ represents the ratio of the ηNN_γ over the πNN_γ coupling strengths.

5. MEASUREMENT OF THE COUPLING RATIOS x_α AND x_γ

As $N_\alpha(u)$ goes through zero at $u_o = 0.1$ GeV^2, the measured ratio $R(u_o)$ determines directly the value of $|x_\gamma|^2$; it is roughly 1 ± .3 and rather insensitive to the exact position u_o. With $x_\gamma = 1 \pm .15$ fixed, we are left with one free parameter, x_α, which determines the expression

$$R(u) = \left| \frac{x_\alpha \cdot x(1)/x(2) N_\alpha(u) - (1 \pm .15)\cdot N_\gamma(u)}{x(1)/x(2) N_\alpha(u) - N_\gamma(u)} \right|^2 \qquad (5)$$

In fig. 7 we show curves R(u) evaluated for various x_α, the other parameters are from line 1 of table 3, and $x_\gamma = 1$. In comparison to the points of measurement, one observes that values of x_α near ±0.5 give a good description whereas values near ±1 do not. The curve labelled 1 in fig. 8 represents $\chi^2(x_\alpha)$, the sum of the squared differences between theory and measurement relative to the errors in table 1. Two clear minima are visible at $x_\alpha = -0.47$ and $x_\alpha = +0.50$ with $\chi^2 = 7.4$ and $\chi^2 = 9.9$ for 8 degrees of freedom. Disregarding negative x^+, the simultaneous fit yields $x_\alpha = 0.52 \pm 0.09$ and $x_\gamma = 0.91 \pm 0.11$. If we multiply N_γ with the factor of equ. (3) (using the coefficients of line 3, table 3), we obtain values that are quite similar: $x_\alpha = 0.50 \pm 0.09$ and $x_\gamma = 0.98 \pm 0.09$. There is a corresponding curve of $\chi^2(x_\alpha)$ labelled 2 in fig. 8.

+ See ref. [15] for a discussion of the relative sign between N_α and N_γ.

As one does not know the definitive form of the amplitude, we think that the final result should contain both sets inside its errors. Therefore, we state as our final result for the ratio of the $\eta NN_\alpha/\pi NN_\alpha$ and $\eta NN_\gamma/\pi NN_\gamma$ couplings measured under the assumption of N_α plus N_γ exchange:

$$x_\alpha = 0.51 \pm 0.10 \qquad \text{and} \qquad x_\gamma = 0.94 \pm 0.13$$

x_α corresponds to $G^2_{\eta NN}/G^2_{\pi NN} = 0.26 \pm 0.10$. As one observes from fig. 7 and from the χ^2 curves, values of x_α as high as required by Heisenberg are completely excluded by the data as long as a linear superposition of N_α and N_γ is taken to describe the $\Lambda\eta$ and $\Lambda\pi^o$ channels.

6. INTERPRETATION OF COUPLING RATIOS IN TERMS OF SU_3

If the ηNN and πNN couplings are SU_3-invariant, there is the ratio $\alpha = D/(F+D)$ to be determined from each x_α or x_γ according to the formula

$$x = (3-4a)/\sqrt{3} \ .$$

We calculate

$$\alpha(N_\alpha) = 0.53 \pm 0.04 \qquad \text{and} \qquad \alpha(N_\gamma) = 0.34 \pm 0.06 \ .$$

It is very interesting to compare these D/(F+D) ratios valid in the space-like region of the N_α and N_γ trajectories with the corresponding ones valid in the time-like region. These were determined by Plane et al. [17] who compared the many different decay widths of the $N^-_{3/2}$ nonet and of the $N^+_{5/2}$ nonet. They found SU_3 invariance, with

$$\alpha(N^+_{5/2}) = 0.55 \pm 0.04 \qquad \text{and} \qquad \alpha(N^-_{3/2}) = 0.31 \pm 0.09 \ .$$

A picture of great consistency has evolved: Fig. 9 shows the two trajectories N_α and N_γ together with the parameters α determined in different points along the trajectories. For each trajectory, α comes out to be the same, independent of u. This is a great success of the Regge model with SU_3 invariant couplings. It implies the <u>small</u> ηNN_α coupling between $u = -1.1$ and $u = +2.8$ GeV^2, and therefore also at the nucleon.

Furthermore it may be noted that the ratios $y_\alpha = x(1)/x(3) = 0.380$ and $y_\gamma = x(2)/x(4) = 0.473$ are equal to 1/3 of the ratio of the $K\Lambda N_\alpha/\pi NN_\alpha$ and $K\Lambda N_\gamma/\pi NN_\gamma$ couplings. If SU_3-invariant, the corresponding D/(F+D) values are calculated according to the formula

$$y = (3-2\alpha)/(3\sqrt{3}) \ .$$

We find[+]

$$\alpha(N_\alpha) = 0.51 \pm 0.10 \quad \text{and} \quad \alpha(N_\gamma) = 0.27 \pm 0.12 \ .$$

This is in remarkable agreement with the previous determinations.

The general consistency one finds for the SU_3 invariant coupling ratios on the N_α and N_γ trajectories supports at the same time the model which describes with a linear superposition of N_α and N_γ what is going on in the $\Lambda\eta$, $\Lambda\pi$ and $(N\pi)_{1/2}$ channels.

7. EXCLUSION OF LARGE ηNN_α COUPLING FOR MORE GENERAL BACKGROUND

In fact the background to N_α does not even have to be the N_γ trajectory in order to exclude the large η coupling. If we only assume that the background B(u) has the same u-dependence in the $\Lambda\eta$ and $\Lambda\pi^o$ channels so that

$$R(u) = \left| \frac{x_\alpha^\eta \cdot N_\alpha(u) + x_B^\eta \cdot B(u)}{x_\alpha^\pi \cdot N_\alpha(u) + x_B^\pi \cdot B(u)} \right|^2$$

then, with $x_B^\eta = x_B^\pi$ and $x = x_\alpha^\eta / x_\alpha^\pi$, this can be written as

$$R(u) = \frac{|x + f(u)|^2}{|1 + f(u)|^2}$$

[+] As the ratios y are based on several $\pi N \to N\pi$ and $K^- p \to \Lambda\pi^o$ experiments, we have assigned an overall normalization error of 10% to y_α and y_γ, or 20% in the cross-sections

where the complex function f(u) represents the ratio of the background over the N_α amplitude. For x near unity, R(u) would have to be near unity as well, contrary to observation. From $R \lesssim 0.4$ for $-u \gtrsim 0.6$ GeV^2 one may conclude that x cannot be larger than 0.8 if it is positive[+]; if |x| is to be larger than 0.8, x would either have to be negative or complex.

8. CONCLUSION

With regard to the value of the ηNN coupling we summarize the situation as follows: With the small value of $G^2_{\eta NN}/G^2_{\pi NN} = 0.26 \pm 0.10$, we have a very satisfactory picture of SU_3 invariant octet couplings on the N_α trajectory, and similar consistency on N_γ, using an $N_\alpha + N_\gamma$ exchange model which describes simultaneously $(\pi N \to N\pi)_{\frac{1}{2}}$ and $K^- p \to \Lambda\pi^o$, $\Lambda\eta$. The observed differential cross-section ratio of $K^- p \to \Lambda\eta$ and $\Lambda\pi^o$ is incompatible with Heisenberg's large ηNN coupling as long as the nucleon Regge trajectory N_α plays the dominant rôle in the $K^- p \to \Lambda\pi^o$ reaction.

ACKNOWLEDGMENTS

This epxeriment was the last one of a series done with the CERN-Munich Spectrometer at the PS. We thank the other members of our group, especially B. Hyams, G. Lutz and P. Weilhammer for their contributions to the construction of the spectrometer.

[+] This conclusion is not valid if f is near -1. A more detailed study of the expression reveals that in order for positive x to be larger than 0.8, the phase of f would have to be -1 within 5%, which would imply almost complete coherence of B with N_α, not only in the phases, but also in the flip-noflip composition, hence almost zero polarization

REFERENCES

[1] G. Ebel et al., Compilation of Coupling Constants and Low-Energy Parameters, Nucl. Phys. B33 (1971) 317, Sect. 3.3 ii.
G.E. Hite, R.J. Jacob, D.C. Moir, Phys. Rev. D12 (1975) 2677.

[2] W. Heisenberg, Introduction to the Unified Field Theory of Elementary Particles, London, New York, Sidney 1966, Chapter 6.

[3] Landolt-Börnstein I/6, Elementary Particle Properties and Production Spectra (1972), Section 1.3.4; 1.5.5.

[4] E.g. B.T. Feld, Models of Elementary Particles, Waltham, Toronto, London 1969, Chapter 15.

[5] K. Kleinknecht, Weak Decays and CP Violation, talk given at the XVIII. International Conference on High-Energy Physics, London (1974), Rutherford Laboratory, Chilton UK.

[6] R.C. Chase et al., Phys. Letters 30B (1969) 659.

[7] J.P. Boright et al., Phys. Letters 33B (1970) 615.

[8] J.K. Storrow and G.A. Winbow, Nucl. Phys. B53 (1973) 62.

[9] E.L. Berger and G.C. Fox, Nucl. Phys. B26 (1971) 1.

[10] F. Marzano et al., (Amsterdam-CERN-Nijmegen-Oxford Collaboration), Nucl. Phys. B123 (1977) 203.

[11] H. Becker et al., Nucl. Phys. B141 (1978) 48.

[12] G. Blanar et al., Nucl. Instr. and Methods 163 (1979) 349.

[13] J. Gallivan et al., Nucl. Phys. B117 (1976) 269.

[14] Particle Data Group, Review of Particle Properties, Phys. Lett. 75B (1978).

[15] N. Papadopoulos and G. Resele, Nuovo Cim. 39A (1977) 515.

[16] D.P. Owen et al., Phys. Review 181 (1969) 1794.

[17] D.E. Plane et al. Nucl. Phys. 22B (1970) 93.

Table 1

Numbers of events $\pi^o \to \gamma\gamma$ and $\eta \to \gamma\gamma$ observed in each u-interval with $\gamma\gamma$ opening angle between ϕ_{min} -25° and $\phi_{90°}$, and ratio of differential cross sections of $K^- p \to \Lambda\eta$ and $\Lambda\pi^o$. $u_{max}(\Lambda\pi^o) = 0.069$, $u_{max}(\Lambda\eta) = 0.046$ GeV^2. (Column 5 contains the corrections due to gamma counter- and spectrometer-acceptance, column 6 contains the branching ratios into $\gamma\gamma$ and the background subtraction.)

u(GeV^2)	π^o	η	ratio	ratio corr'd	ratio of diff. cross sections
+0.1 - +0.05	27	0	-	-	-
+0.05 - 0	72	8	0.11	0.11	0.27 ± 0.14
0 - -0.05	28	14	0.50	0.43	0.96 ± 0.31
-0.05 - -0.1	29	11	0.38	0.35	0.79 ± .28
-0.1 - -0.2	28	12	0.43	0.42	0.93 ± .33
-0.2 - -0.3	17	8	0.47	0.51	1.14 ± .49
-0.3 - -0.4	25	6	0.24	0.28	0.63 ± .28
-0.4 - -0.6	37	7	0.19	0.21	0.47 ± .19
-0.6 - -0.8	35	3	0.09	0.11	0.24 ± .15
-0.8 - -1.1	18	1	0.06	0.08	0.18 ± .18
+0.1 - -1.1	316	70	0.22		

Table 2

Measured cross-sections and polarizations of the reactions $K^-p \to \Lambda\pi^o$ and $K^-p \to \Lambda\eta$ at 6 GeV/c

u (GeV^2)	$d\sigma/du$ ($\mu b/GeV^2$) $\Lambda\pi^o$	$\Lambda\eta$	P $\Lambda\pi^o$
0.1 - 0.05 [+)]	4.31 ± .94	-	+.26 ± .31
0.05- 0 [+)]	3.00 ± .25	.89 ± .3	-.05 ± .23
0 - -0.05	1.92 ± .21	2.4 ± .7	+.37 ± .28
-0.05- -0.1	1.66 ± .22	1.4 ± .5	-.75 ± .44
-0.1 - -0.2	1.28 ± .12	1.2 ± .4	-.06 ± .37
-0.2 - -0.3	1.09 ± .17	1.05± .4	-.67 ± .51
-0.3 - -0.4	1.72 ± .24	.81 ± .35	-1.01± .44
-0.4 - -0.6	1.96 ± .22	.78 ± .30	-.62 ± .37
-0.6 - -0.8	2.26 ± .28	.36 ± .20	-.83 ± .42
-0.8 - -1.1	1.87 ± .30	.17 ± .17	-.48 ± .55
	Integrated cross-sections [++)]		Ratio
u_{max} - -1.1	2.23 ± .25 μb	.94 ± .19 μb	.42 ± .08

+) $u_{max}(\Lambda\pi) = .069$, $u_{max}(\Lambda\eta) = .046$

++) including the over-all normalization error of ± 10%

u(GeV^2)	P($\Lambda\eta$)
u_{max} - -.1	.20 ± .43
-.1 - -.25	-1.05 ± .65
-.25- -.5	-.02 ± .50

Table 3

Relative contributions x and form factor parameter B of N_α and N_γ Regge poles fitted to the data of fig. 6

Data (GeV/c)	x(1) $(\mu b^{\frac{1}{2}})$	x(2) $(\mu b^{\frac{1}{2}})$	x(3) $(\mu b^{\frac{1}{2}})$	x(4) $(\mu b^{\frac{1}{2}})$	B (GeV^{-2})
$\Lambda\pi^o$(4.2, 5, 6)	692 ± 19	267 ± 18	-	-	-
$(N\pi)_{\frac{1}{2}}$(5.9, 10)	-	-	1820 ± 40	565 ± 80	-
$\Lambda\pi^o$(6)	834 ± 41	67 ± 31	-	-	37 ± 19

Table 4

The two trajectories N_α and N_γ and the octet coupling ratio $\alpha = D/(F+D)$

m^2 or u (GeV^2)	α	method	reference
N_α-trajectory:			
$+2.85(N^+_{5/2})$	0.55 ± 0.04	Fit to strong decay rates	[17]
$+0.88(N^+_{1/2})$	0.657 ± 0.007	Cabbibo fit to weak decays	[5]
	0.61 ± 0.05	$G^2(\Sigma\Lambda\pi)$ from Goldberger-Treiman relation on $\Sigma \to \Lambda e\nu$	[3]
-1 to 0	0.53 ± 0.04	N_α and N_γ exchange in $(K^-p \to \Lambda\eta)/(K^-p \to \Lambda\pi^0)$	this exp.
	0.51 ± 0.10	N_α and N_γ exchange in $(K^-p \to \Lambda\pi^0)/(\pi N \to N\pi)_{\frac{1}{2}}$	this exp. and [16, 7]
N_γ-trajectory:			
$+2.31(N^-_{3/2})$	0.31 ± 0.09	Fit to strong decay rates	[17]
-1 to 0	0.34 ± 0.06	N_α and N_γ exchange in $(K^-p \to \Lambda\eta)/(K^-p \to \Lambda\pi^0)$	this exp.
	0.27 ± 0.12	N_α and N_γ exchange in $(K^-p \to \Lambda\pi^0)/(\pi N \to N\pi)_{\frac{1}{2}}$	this exp. and [16, 7]

Figure captions

Fig. 1: Three graphs useful for the determination of the ηNN coupling.

Fig. 2: a) Schematic of the apparatus,
b) Detail of the target region and trigger counters.

Fig. 3: Distribution of the squared missing mass m_x^2 in the reaction $K^- p \to \Lambda X$.
a) All events,
b) All events with 1,2 or 3 neutral signals,
c) All events with two γ's coplanar with the missing momentum $\vec{p}_x$, and recorded in two different strips of the gamma counter.

Fig. 4: Scatterplots of the events with two coplanar γ's seen in two different strips. Missing mass squared vs. the $\gamma\gamma$ opening angle for each u-interval. The boxes contain 87% of the $\pi^o \to \gamma\gamma$ and $\eta \to \gamma\gamma$ decays.

Fig. 5: Differential cross sections and polarizations for $K^- p \to \Lambda\pi^o$ and $\Lambda\eta$ as functions of the momentum transfer u.

Fig. 6: Comparison of the measured differential cross sections at various energies of $K^- p \to \Lambda\pi^o$ and $\pi N \to N\pi$ ($I_u = \frac{1}{2}$) with an N_α and N_γ Regge exchange model. The curves for each reaction represent a 2-parameter fit with formulae (1),(2) of the text. The broken line represents a 3-parameter fit to the $\Lambda\pi^o$ data at 6 GeV/c only, formula (3).

Fig. 7: Comparison of the measured ratio $d\sigma/du$ ($\Lambda\eta$) over ($\Lambda\pi$) with the calculated curves of equ. 5 for 7 different values of the coupling constant ratio x_α. x_α near ± 0.5 is favoured. The N_α, N_γ pole model of ref. [15] was used.

Fig. 8: χ^2 profiles of the coupling ratio x_α for two fits of R(u) to formulae (4). Curve 1: using the original N_α, N_γ pole model of ref. [15].

Figure captions (cont'd.)

Curve 2: using a modification of N_γ. In both cases, the smaller, SU_3 compatible, values are preferred, and the larger values required by Heisenberg are excluded.

Fig. 9: SU_3 parameter $\alpha = D/(F+D)$ on the nucleon Regge trajectories N_α and N_γ. For each trajectory there is a universal value of α in the timelike and spacelike regions. Note that the quark model gives $\alpha = 3/5$ for N_α and $\alpha = 3/8$ for N_γ.

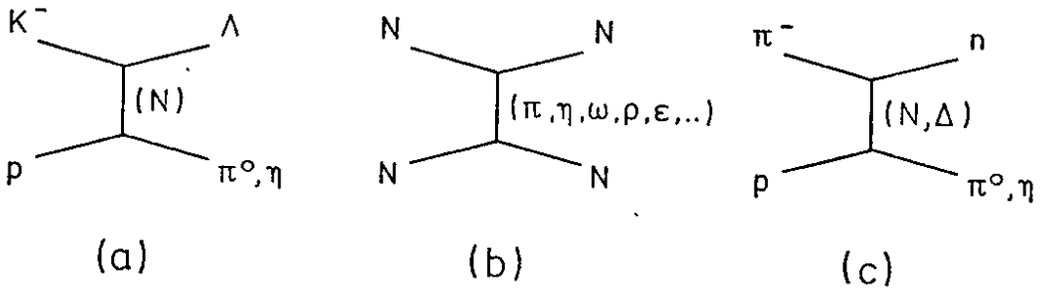

Fig. 1

C = Cerenkov Counter P = Proportional Chambers H_2 = Liquid Hydrogen
S = Spark Chambers Fe = Iron Shielding L = Trigger Counter
F = $A_{1,2}$ = Veto Counters

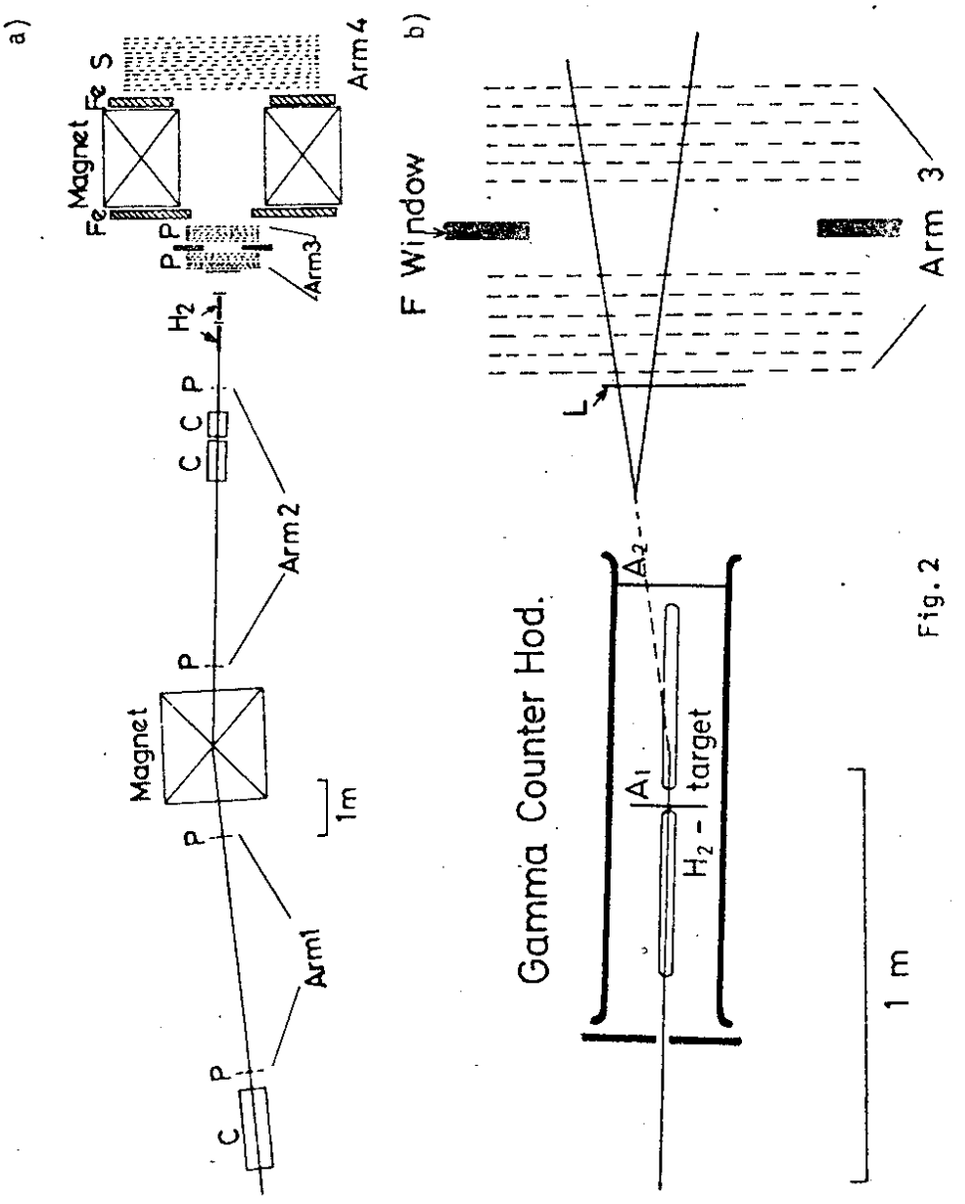

Fig. 2

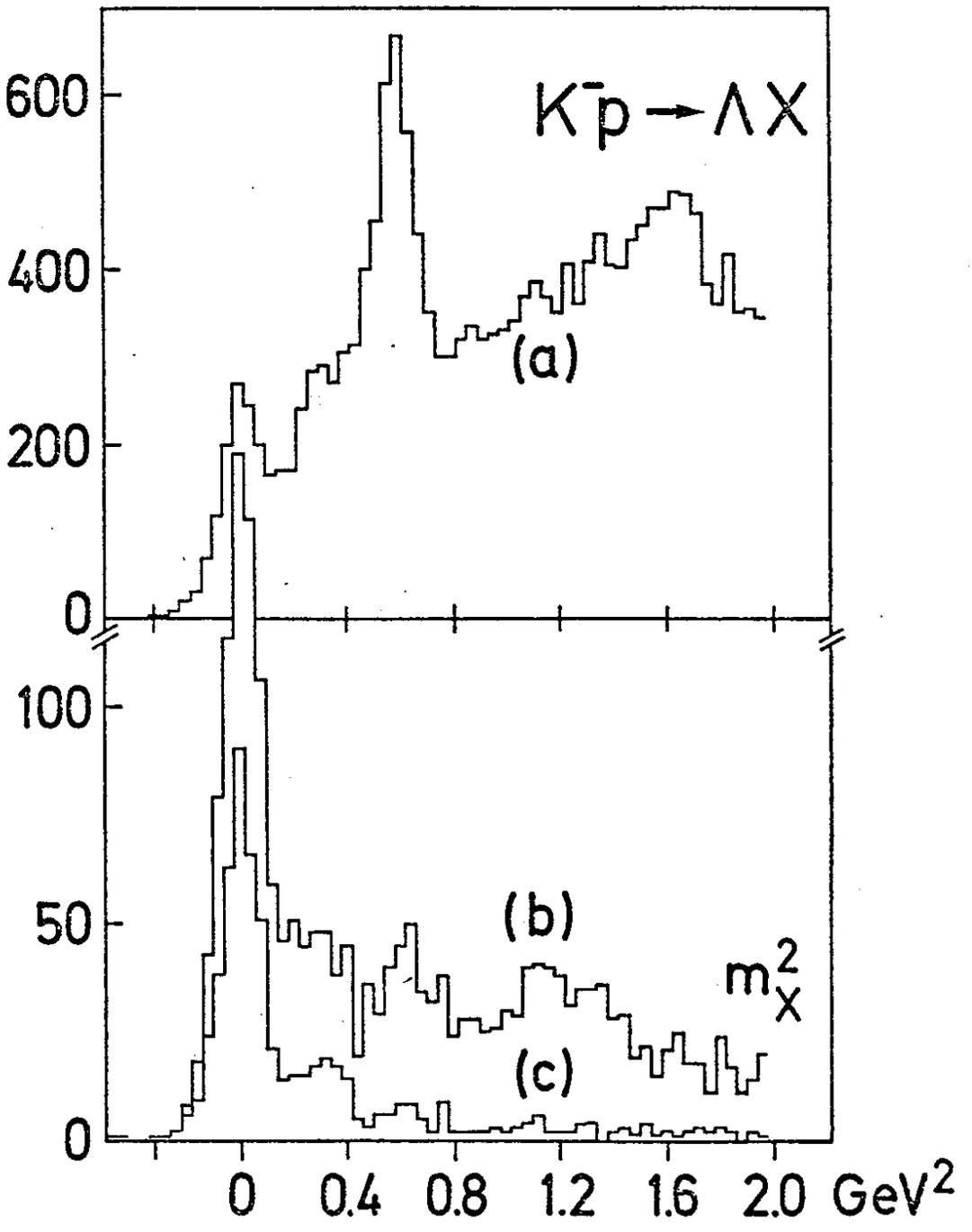
600
400
200
0
$K^-p \rightarrow \Lambda X$
(a)
100
50
0
(b)
(c)
m_X^2
0
0.4
0.8
1.2
1.6
2.0
GeV^2

Fig.3

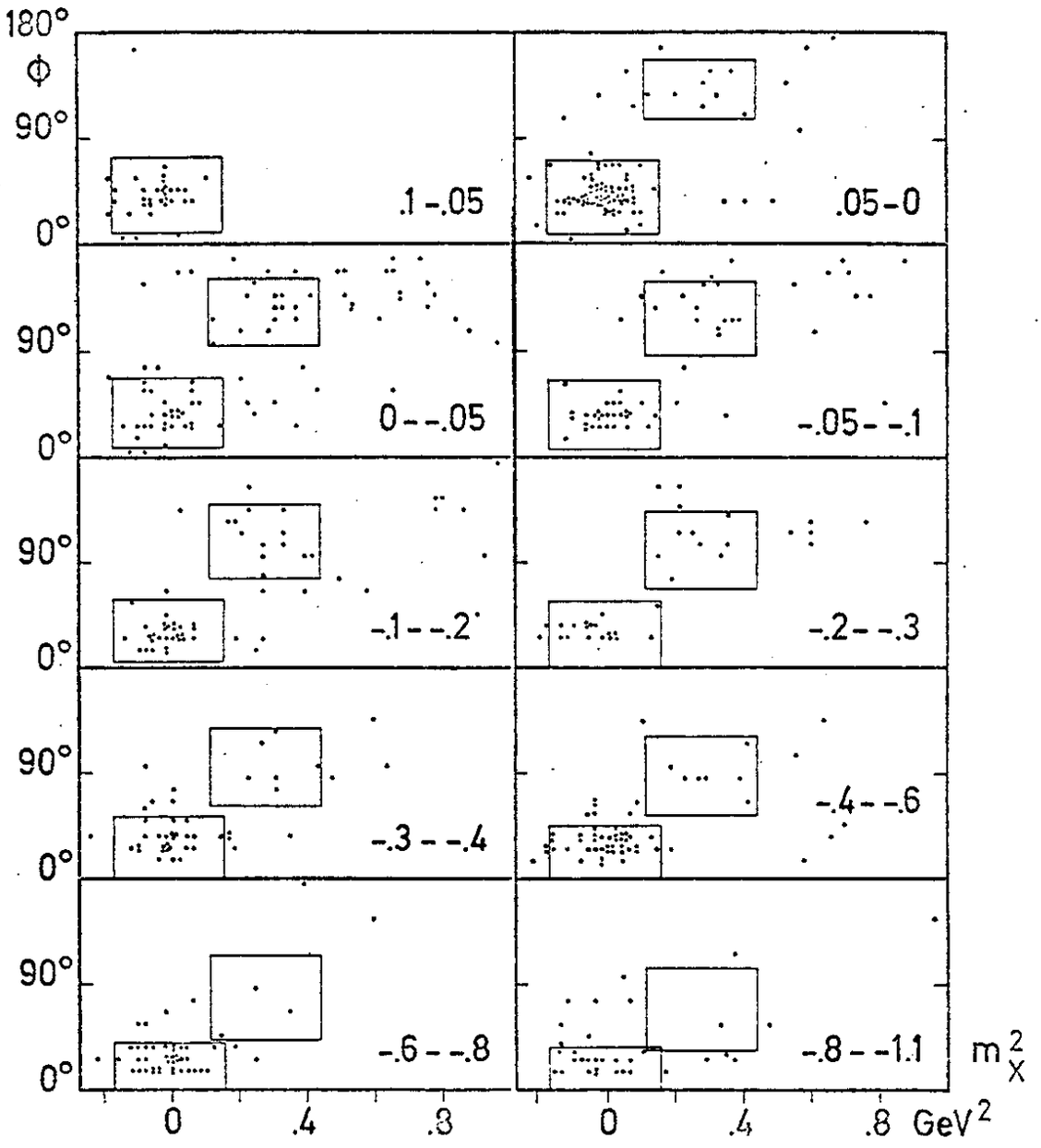

Fig.4

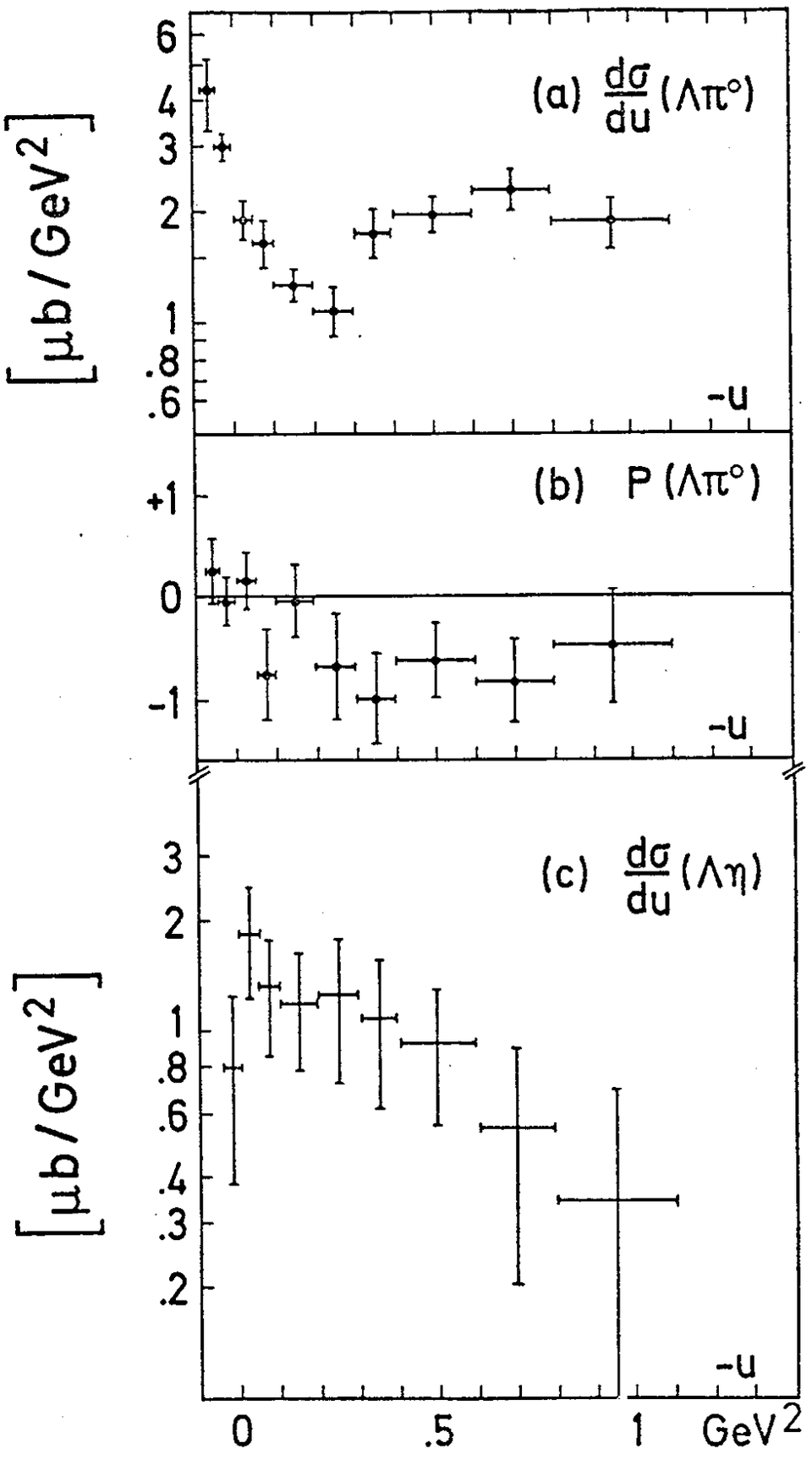
[μb/GeV²]
6
4
3
2
1
.8
.6
(a) dσ/du (Λπ°)
-u
(b) P (Λπ°)
+1
0
-1
-u
[μb/GeV²]
3
2
1
.8
.6
.4
.3
.2
(c) dσ/du (Λη)
-u
0
.5
1
GeV²

Fig. 5

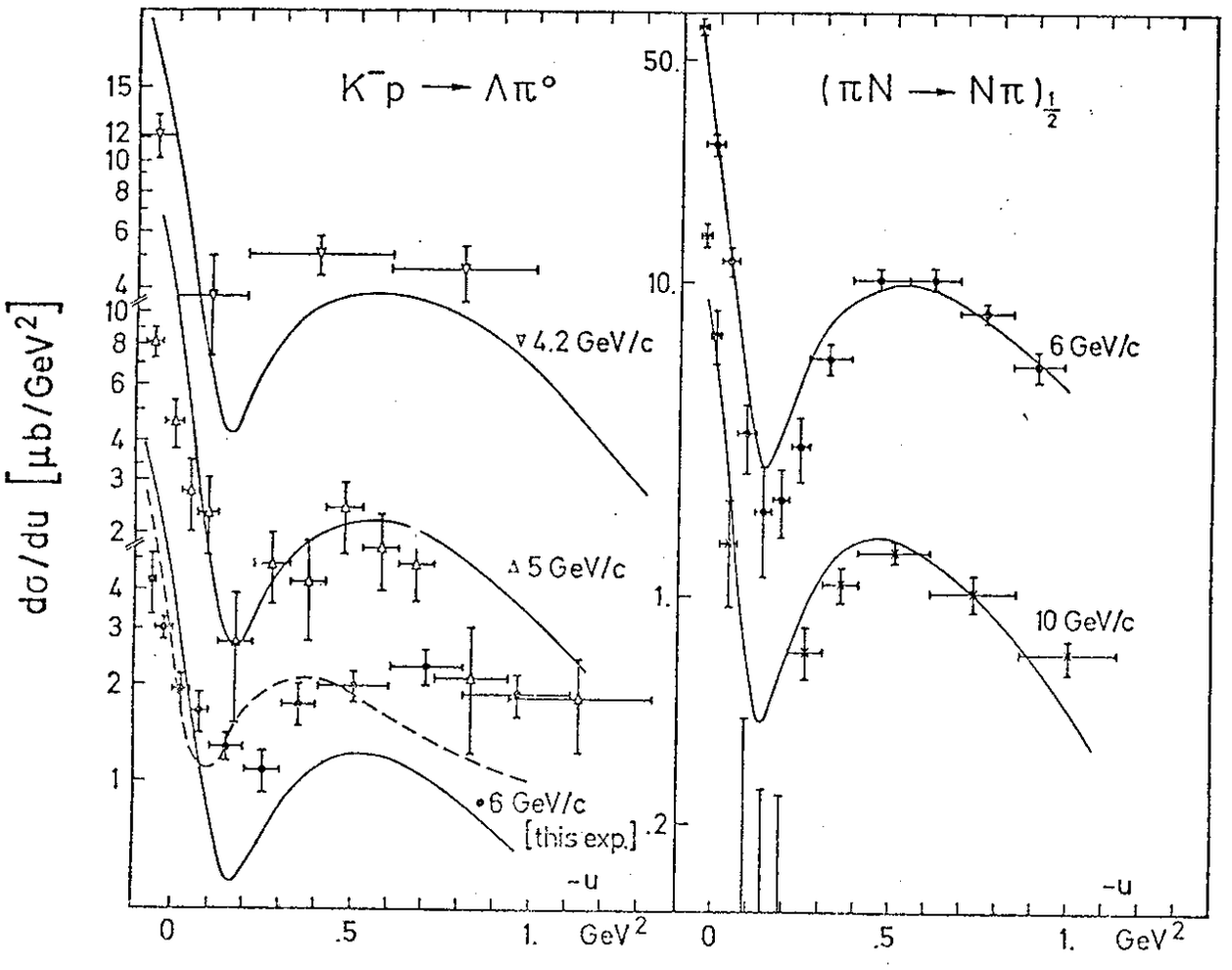
$K^-p \rightarrow \Lambda\pi^\circ$
$(\pi N \rightarrow N\pi)_{\frac{1}{2}}$
$d\sigma/du$ [μb/GeV^2]
▽ 4.2 GeV/c
△ 5 GeV/c
• 6 GeV/c
[this exp.]
6 GeV/c
10 GeV/c
-u
GeV^2

Fig.6

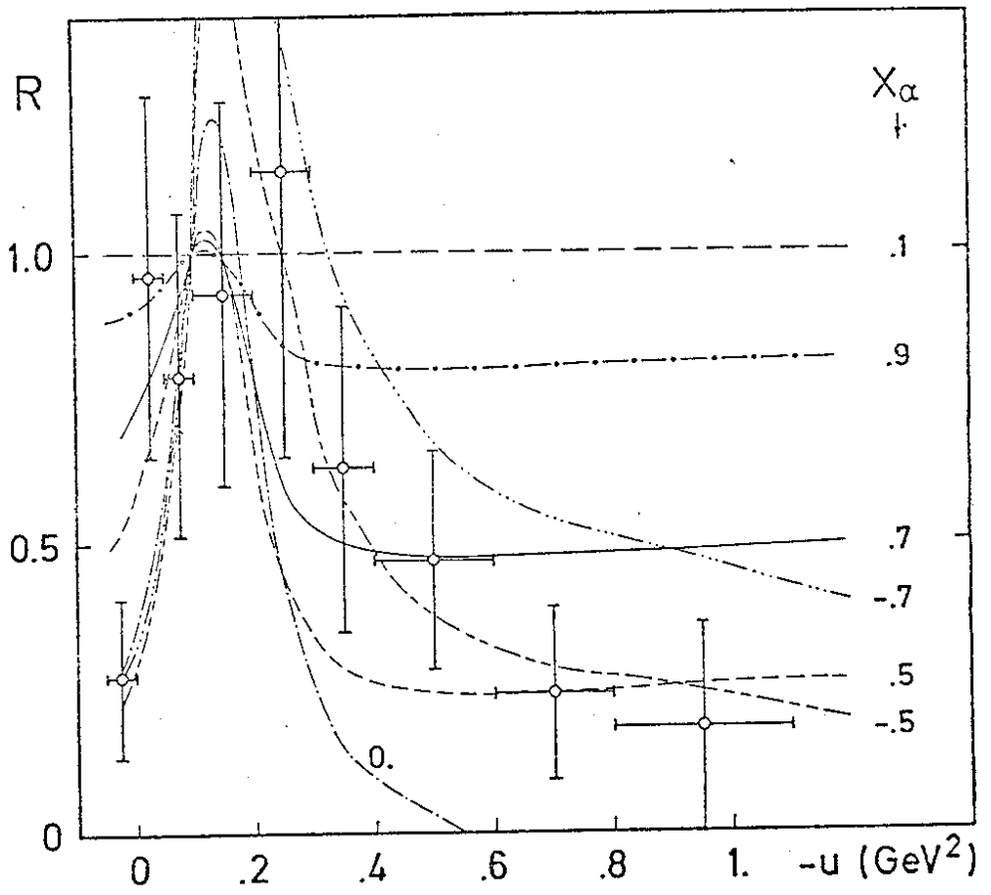
R
X_α
1.0
0.5
0
.1
.9
.7
-.7
.5
-.5
0.
0
.2
.4
.6
.8
1.
-u (GeV^2)

Fig.7

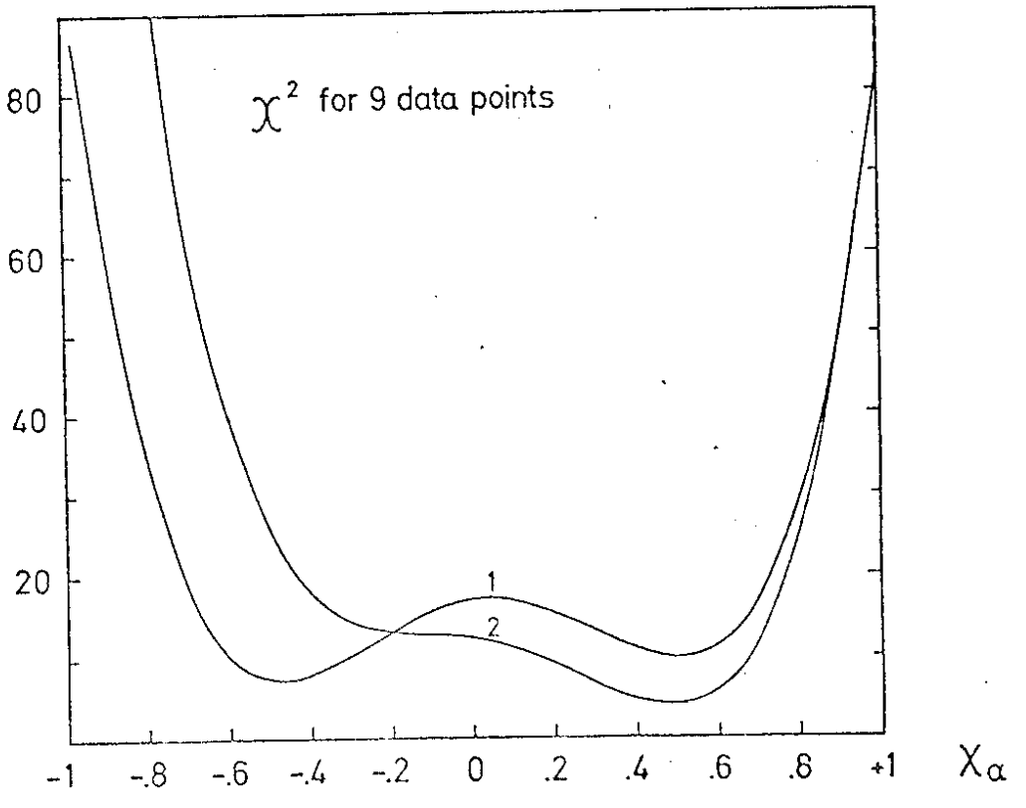
χ^2 for 9 data points
80
60
40
20
1
2
-1
-.8
-.6
-.4
-.2
0
.2
.4
.6
.8
+1
X_α

Fig.8

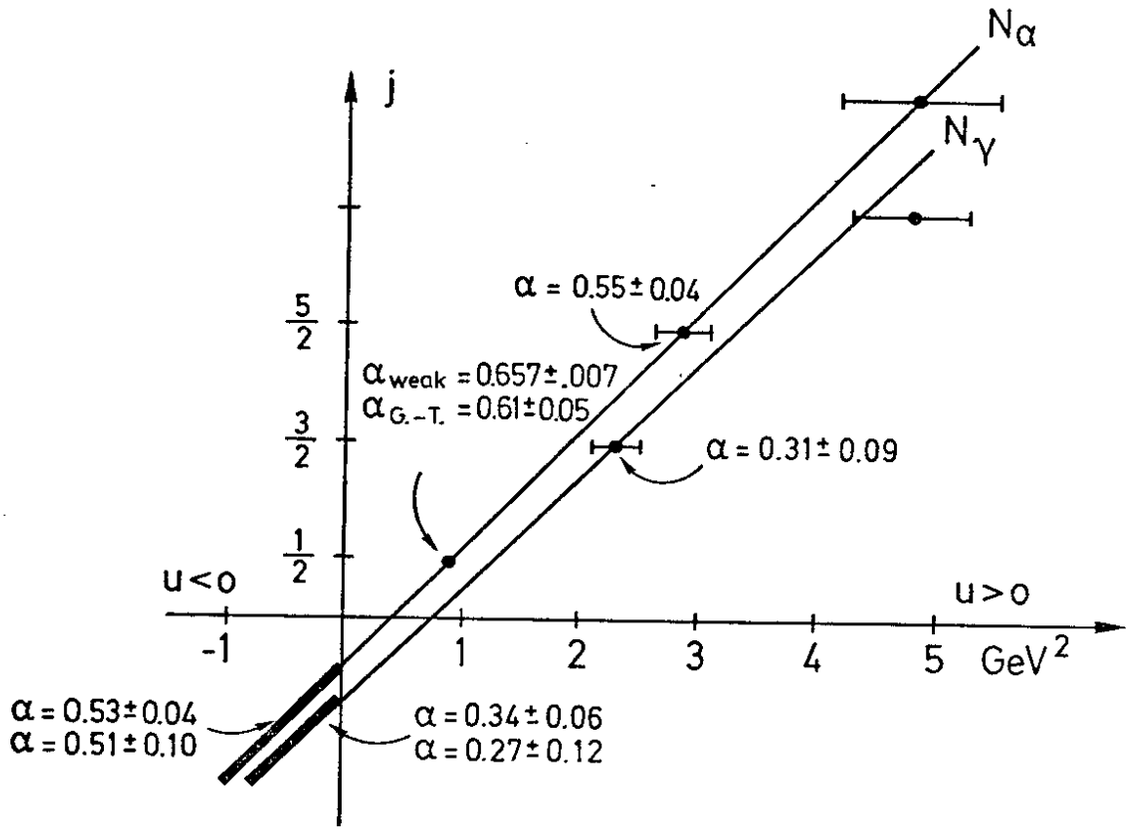
Nα
Nγ
j
α = 0.55 ± 0.04
5/2
αweak = 0.657 ± .007
αG.-T. = 0.61 ± 0.05
3/2
α = 0.31 ± 0.09
1/2
u<o
u>o
-1
1
2
3
4
5
GeV²
α = 0.53 ± 0.04
α = 0.51 ± 0.10
α = 0.34 ± 0.06
α = 0.27 ± 0.12

Fig. 9

Druck: Dokumentation Astrophysik Karl-Schwarzschild-Str. 1 · 8046 Garching bei München